Materials Science and Engineering A 527 (2010) 5092–5099

Contents lists available at ScienceDirect

Materials Science and Engineering A

journal homepage: www.elsevier.com/locate/msea

Hardening and microstructural reactions in high-temperature equal-channel angular pressed Mg–Nd–Gd–Zn–Zr alloy

G. Sha[a,b,*], J.H. Li[b,c], W. Xu[d], K. Xia[d], W.Q. Jie[c], S.P. Ringer[a,b]

[a] ARC Centre of Excellence for Design in Light Metals, The University of Sydney, NSW 2006, Australia
[b] Australian Centre for Microscopy & Microanalysis, The University of Sydney, NSW 2006, Australia
[c] State Key Laboratory of Solidification Processing, Northwestern Polytechnical University. Xi'an 710072, China
[d] Department of Mechanical Engineering and ARC Centre of Excellence for Design in Light Metals, University of Melbourne, Victoria 3010, Australia

ARTICLE INFO

Article history:
Received 19 January 2010
Received in revised form 7 March 2010
Accepted 19 April 2010

Keywords:
Mg alloy
Equal-channel angular pressing
Precipitation
Strengthening
Nucleation and growth

ABSTRACT

The use of high-temperature (330 °C) equal-channel angular pressing (ECAP) is demonstrated to promote precipitation of a fine and uniform dispersion of the FCC β_1 phase in an Mg–Nd–Gd–Zn–Zr alloy. Significantly, this process induces a hardening reaction in the alloy, where isothermal ageing at this temperature leads only to softening. The evolution of microstructure is characterized using transmission electron microscopy and scanning electron microscopy. The nucleation and growth of precipitates during the high-temperature ECAP are discussed. This research highlights a new approach to engineer precipitate microstructures via the application of severe plastic deformation so as to extend the property space of high-temperature Mg alloys.

1. Introduction

Magnesium alloys containing rare earth (RE) elements have received significant recent attention because they exhibit a strong age-hardening response and good creep resistance [1–6]. In particular, the RE-modified Mg alloys exhibit improved high-temperature performance when compared with conventional Mg alloys and are able to withstand service temperatures up to ~250 °C [7,8]. Already, these materials are being used in the aircraft industry [7] and the high-temperature properties of these alloys have generated significant interest as potential materials for jet engine applications [1]. A wide range of Mg-RE alloys have now been investigated to explore their age-hardening response and precipitation sequences [1–9]. The Mg–Nd–Gd–Zn–Zr alloys seem particularly attractive because they exhibit a stronger hardening response with lower overall RE levels [5]. Two modes of precipitation reaction have been reported in these alloys, depending on the ageing temperature. Below ~200 °C, ageing produces a high strengthening effect due to the formation of a fine and uniform dispersion of β″ precipitates (DO_{19} hexagonal; $a = b = 0.64$ nm and $c = 0.52$ nm [5]) and β′ precipitates (base-centred orthorhombic; $a = 0.640$ nm, $b = 2.223$ nm, $c = 0.521$ nm) [5]. The metastable β″ and β′ phases are unstable at ageing temperatures above 300 °C and the β_1 phase (FCC; space group $Fm\bar{3}m$, $a = 0.73$ nm [6]) precipitates directly from the solid solution, instead. It has been a challenge to optimize the dispersion of fine β_1 precipitates because these precipitates exhibit low nucleation rates and rapid growth during conventional ageing treatments at 300 °C. There is great interest to develop new approaches to boost the nucleation and restrict the growth of β_1 precipitates in Mg-RE alloys in order to improve the alloy strength at high temperatures.

Severe plastic deformation (SPD) is well known to be effective in modifying microstructure and creating a unique balance of properties. Equal-channel angular pressing (ECAP) is an attractive SPD method because it can produce ultrafine-grained microstructures and has potential for scale-up and mass production [10–12]. As might be expected, initial studies have demonstrated that low-temperature SPD leads to more pronounced grain refinement than the high-temperature variant and most SPD experiments tend to be conducted at lower temperatures [10–17]. It is also well known that ultrafine-grained microstructures often exhibit poor stability at higher temperatures [18–21] and are therefore not amenable to high-temperature service applications. High-temperature SPD as an alternative can be attractive if it can successfully modify precipitate microstructure for better strengthening effect in Mg-RE alloys. To our knowledge, there are no reports yet available on the

* Corresponding author at: Australian Centre for Microscopy and Microanalysis, The University of Sydney, NSW 2006, Australia. Tel.: +61 2 90369050; fax: +61 2 93517682.
E-mail address: gang.sha@sydney.edu.au (G. Sha).

0921-5093/$ – see front matter.
doi:10.1016/j.msea.2010.04.064

effects of high-temperature SPD on the hardening and microstructure in Mg-RE alloys and the opportunity for dynamic modification of the precipitation processes. More recently, there has been growing interest in using SPD to control precipitation microstructures so as to achieve a combination of strengthening from *both* grain refinement and precipitation hardening [22–24] and SPD was recently demonstrated as effective in modifying precipitate microstructures in Al–Zn–Mg–Cu alloys [25].

In this research, we investigate the use of ECAP to modify high-temperature precipitate microstructure in order to strengthen Mg-RE alloys. A two-step ECAP procedure was devised to refine the precipitate microstructure of an Mg–Gd–Nd–Zn–Zr alloy and improve its strength for high-temperature applications. Careful microscopy experiments were performed to characterize the resultant multi-scale microstructures of the Mg-RE alloy. This paper presents a detailed overview of the evolution of precipitate microstructure and for the first time address the nucleation and growth of precipitates in the alloy during ECAP processing at 330 °C.

2. Experimental material and procedures

The Mg–2.58Nd–1.80Gd–0.60Zn–0.15Zr (wt.%) alloy was prepared from high purity Mg (99.9 wt.%), Zn (99.9 wt.%), Nd (99.9 wt.%), and Mg–28Gd (wt.%) and Mg–33Zr master alloys in an electrical resistance furnace under the protection of an anti-oxidizing flux before being cast into a sand mould to form rods of 10 mm diameter and 200 mm length. These as-cast rods were cut into short billets having lengths of 50 mm. Solution heat treatment was performed on the billets in a salt bath at 520 °C for 18 h, followed by quenching into cold water. To refine the microstructure of the cast rods after solution treatment, the samples were subjected to a two-step high-temperature ECAP process. Firstly the billets were given 4 ECAP passes at 350 °C. These samples were again solution treated at 520 °C for 20 h, followed by water quenching and we designated this as the as-quenched (AQ) condition of the alloy. A second ECAP stage was subsequently performed at 330 °C for 1 pass and 8 passes, corresponding to an imposed strain of ~1 and ~8, respectively [26]. For each ECAP experiment, samples were inserted into a pre-heated 90° die and held at temperature for 15 min before pressing. Processing *route C* was used in all pressings [27] under a back pressure of 100 MPa. The pressing speed was 5 mm/min, resulting in a pressing time of about 10 min for one pass and 75 min for 8 passes. To provide a comparison of the effect of ageing, two billets in the AQ condition were aged at 330 °C for 30 and 90 min, which is approximately equivalent to the processing times for 1-pass and 8-pass second stage ECAP, respectively.

Vickers hardness testing was performed using a LECO Hardness Tester (LV700AT) with a 5 kg load and 15 s dwell time. Each data point represented an average of at least 10 measurements. Disks of 3 mm diameter were punched from thin strips cut from the ECAP samples and these were ground carefully to a thickness of ~100 μm before being twin-jet electropolished into thin foils for transmission electron microscopy (TEM) using standard techniques [6]. Our TEM examinations were performed using a Philips CM12 operating at 120 kV. We also examined polished cross-sections using a Zeiss ULTRA scanning electron microscope (SEM) operating at 2 kV. Optical microscopy was performed using an Olympus TIRF (total internal reflection fluorescence) Microscope in a normal reflection mode.

3. Results

3.1. Hardening responses of an Mg–Nd–Gd–Zn–Zr alloy processed by different routes

Fig. 1 shows that processing by isothermal ageing at 330 °C produces a very different hardening response in the as-quenched (AQ) Mg–Nd–Gd–Zn–Zr alloy from processing by ECAP at the same temperature. The ageing treatments at 330 °C up to 90 min did not produce any significant strengthening effect in the alloy, indicating that the alloy had a poor hardening response during ageing at the temperature. In contrast, a marked hardening effect from an initial value of 60 to a value of 73 Hv was evident in the alloy after processed by 1-pass ECAP at 330 °C (with a processing time of 30 min). After 8-pass ECAP processing (with a processing time of 90 min), the hardness of the alloy decreased slightly to a value of 68 Hv. The hardness decrease is mainly due to the coarsening of precipitates because coarse spherical precipitates in low number density were observed from microstructure characterizations.

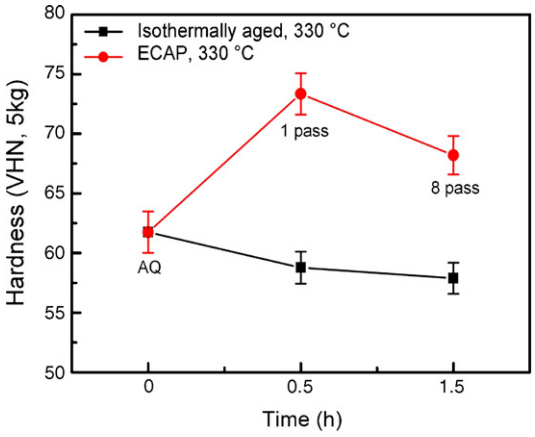

Fig. 1. Age-hardening curves for Mg–2.58Nd–1.80Gd–0.60Zn–0.15Zr alloy under ECAP and isothermal ageing treatment at 330 °C.

3.2. Microstructural changes from solution treatments and 4-pass ECAP processing

The as-cast Mg–Nd–Gd–Zn–Zr alloy samples were given a series of pre-treatments including a solution treatment, 4-pass ECAP processing at 350 °C and the second solution treatment to reduce non-uniformity of casting microstructure. Fig. 2a is a light optical micrograph of the microstructure of the as-cast alloy, which comprised equiaxed α-Mg grains surrounded by eutectic regions. The mean grain size was measured to be approximately 100 μm using a linear intercept method. Large particles of a secondary phase were evident at the grain boundary regions. After solution treatment at 520 °C for 18 h, the eutectic structures were dissolved, but the large secondary phase particles remained at the boundaries, Fig. 2b. The mean grain size was unchanged after the solution treatment. A fine grey contrast was observed inside each grain, Fig. 2b, and these were precipitates formed during cooling from the solution treatment. These coarse precipitates were thought to be $ZnZr_2$, which are frequently observed in similar alloys after solution treatment [5]. A further microstructural refinement was imparted to these ingots following a 4-pass ECAP at 350 °C and a second solution treatment at 520 °C for 20 h. As noted earlier, we refer to this as the AQ microstructure and it is seen to exhibit equiaxed grains with a mean grain size of approximately 50 μm in the inverted SEM image provided in Fig. 2c. Significantly fewer coarse particles were observed at the grain boundaries in this AQ condition.

3.3. Microstructural evolution during isothermal ageing at 330 °C

Isothermal ageing treatments were performed on the as-quenched samples at 330 °C (the same temperature used for ECAP processing) with an objective to reveal the pure static ageing effect on the microstructure of the alloy. The isothermal ageing at 330 °C

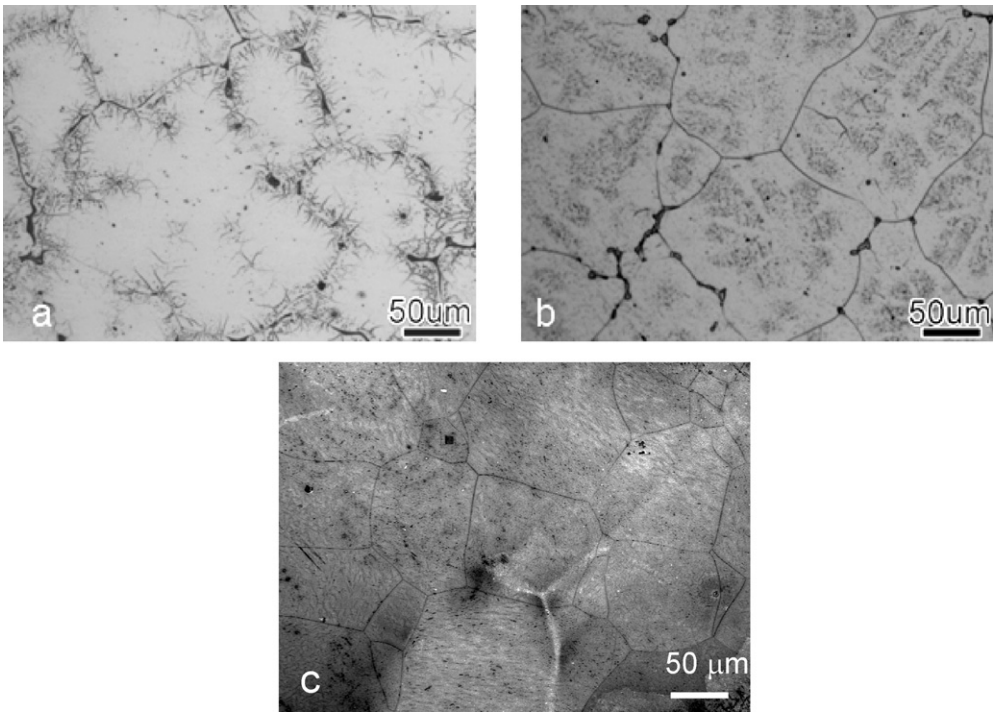

Fig. 2. Microstructures of Mg–2.58Nd–1.80Gd–0.60Zn–0.15Zr alloy samples in the (a) light optical image of as-cast condition, (b) light optical image after solution treatment at 520 °C for 18 h, and (c) secondary electron image (after contrast reversal) of alloy processed by ECAP for 4 passes at 350 °C followed with a solution treatment at 520 °C for 20 h.

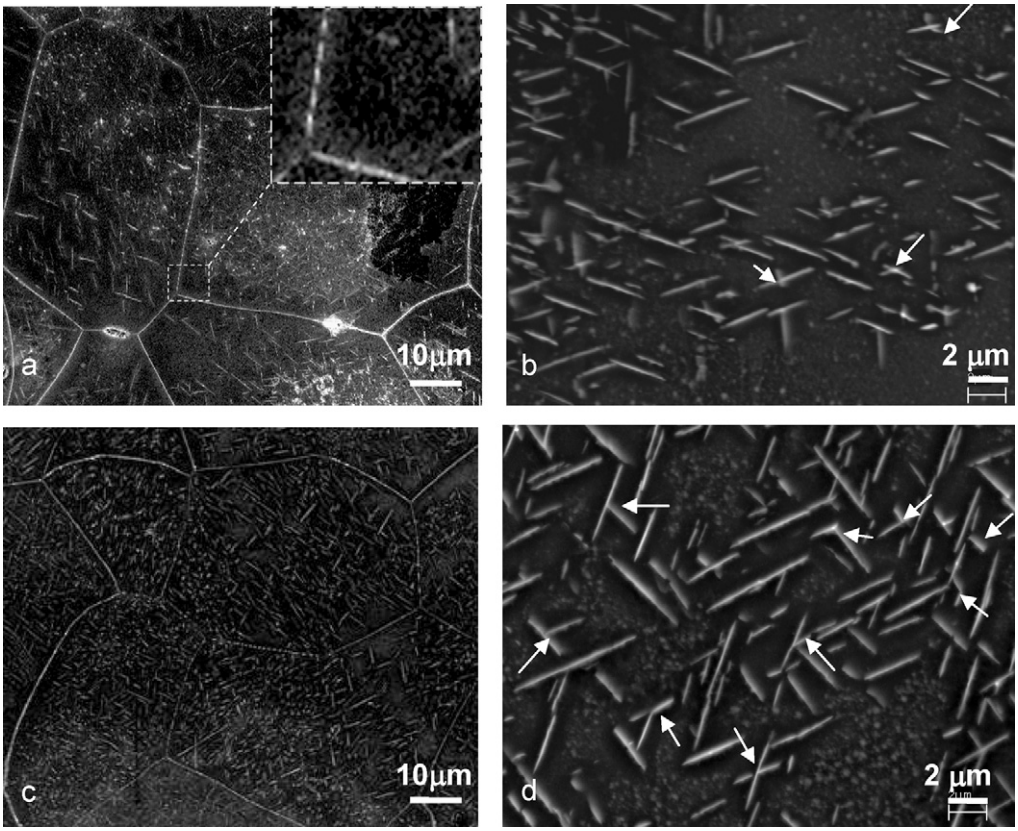

Fig. 3. Scanning electron micrographs of Mg–2.58Nd–1.80Gd–0.60Zn–0.15Zr alloy samples aged isothermally at 330 °C for (a and b) 30 min and (c and d) 90 min.

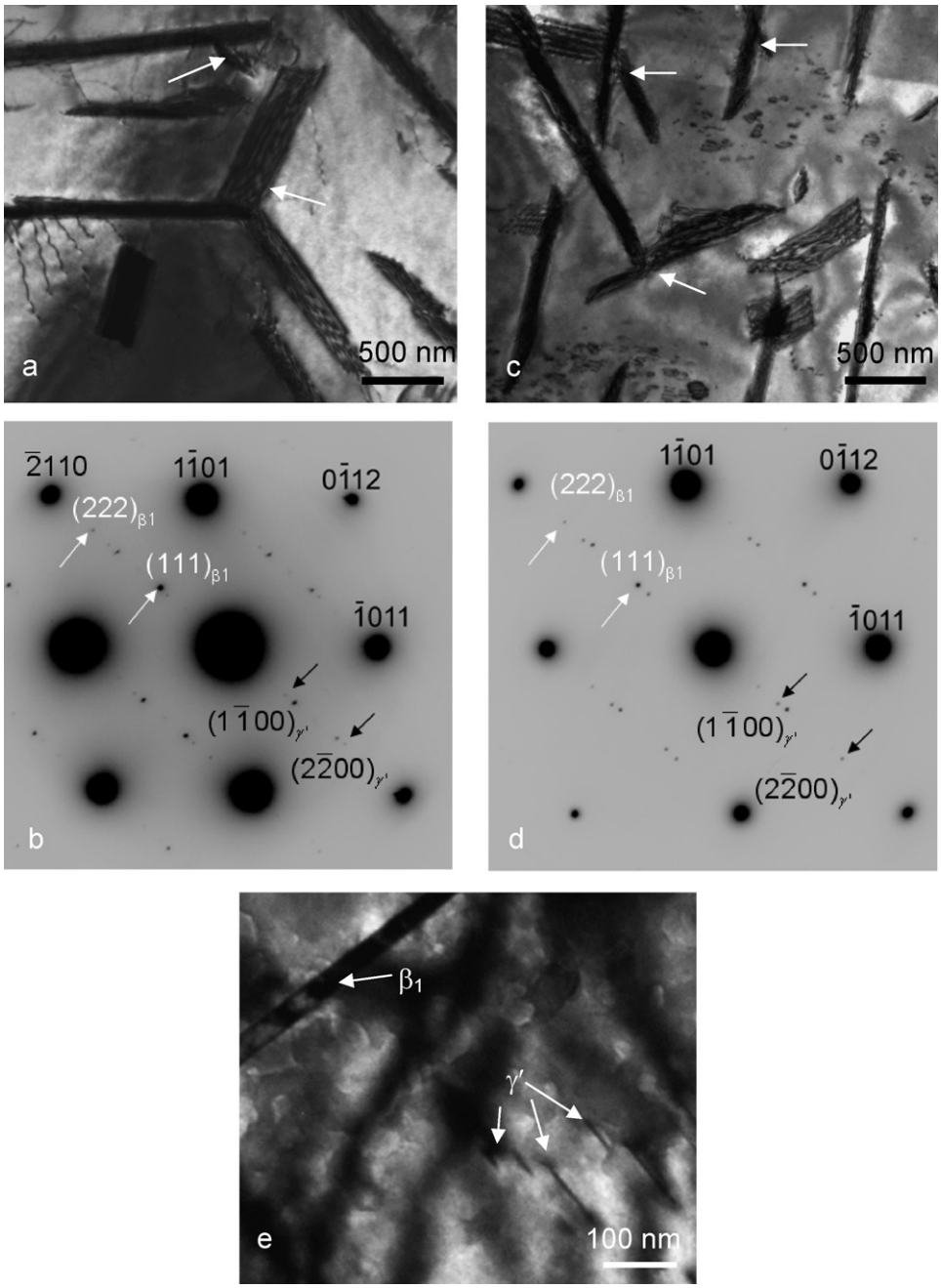

Fig. 4. TEM results from samples isothermally aged at 330 °C (a) $[0\,1\,\bar{1}\,1]_{\alpha\text{-Mg}}$ bright field image and (b) corresponding SAED pattern from the alloy after 30 min ageing, (c) bright field image, (d) SAED pattern from the alloy after 90 min ageing, and (e) $[1\,0\,\bar{1}\,0]_{\alpha\text{-Mg}}$ bright field image of a sample aged for 90 min.

caused no change to the mean grain size of the alloy samples, Fig. 3. A coarse dispersion of large elongated precipitates with length between 1 and 5 μm was observed in the microstructure of samples aged for 30 min at 330 °C, Fig. 3a and b. The grain boundaries, as shown in the inset of Fig. 3a, were decorated with precipitation. Some boundaries were decorated with a chain of discontinuous elongated particles. These particles appeared parallel with each other, with their long axis at a small angle to the grain boundary. Other boundaries were decorated with a continuous grain boundary precipitate phase. These inter and intra-granular precipitates were identified as β_1 using electron diffraction analyses and this is discussed in more detail, below. After further ageing for 90 min at 330 °C, the number density of the β_1 precipitates appeared unchanged, but the growth of these elongated precipitates were evident in Fig. 3c and d, with largest β_1 precipitates grown to approximate 7 μm in length. Nevertheless, as it is clear from the data in Fig. 1, the formation of coarse β_1 precipitate microstructure offered relatively little strengthening effect.

Bright field (BF) TEM micrographs and corresponding selected area electron diffraction (SAED) patterns recorded from alloy samples aged at 330 °C both for 30 and 90 min along $[0\,1\,\bar{1}\,1]_{\text{Mg}}$ are provided in Fig. 4a–d. The SAED patterns contained two sets of precipitate reflections in addition to the Mg-matrix diffractions. One set of these diffractions was annotated with white arrows between the central spot and the $(\bar{2}\,1\,1\,0)_{\text{Mg}}$ reflection and these were indexed as consistent with the β_1 precipitate with the same orientation relationships in the Mg matrix as reported in Ref. [6]. These corresponded to the plate-shaped precipitates of length between 0.2 and 2 μm as seen in Fig. 4a and c, and both ageing conditions include examples where there seem to be β_1 precipi-

tate intersections, indicated by arrows. Another set of precipitate diffractions at 1/3 and 2/3 g $(2\bar{1}\bar{1}0)_{Mg}$, as shown in Fig. 4b and d, were indexed as consistent with the γ′ phase (MgZnRE containing, hexagonal, $a = 0.55$ nm, $c = 0.52$ nm [1,28]). This suggestion is consistent with observation of basal precipitate plates (<100 nm long, ~4 nm thick) in view directions close to $[10\bar{1}0]_{\alpha\text{-Mg}}$ as shown in Fig. 4e. These reflections were stronger in the sample aged 90 min and this is consistent with reports of the sluggish kinetics of γ′ precipitation [28]. The only difference between the two SAED patterns in Fig. 4b and d was the relative intensities of the two sets of precipitate reflections. The presence of both β-type and γ-type of precipitates in the isothermally aged samples is consistent with previous work on Mg–3 wt.% Nd(–Zn) alloys [29]. Overall, it was clear that the diffraction effects from β_1 were stronger than those from γ′, indicating that β_1 was the dominant precipitate phase in both conditions. This is likely due to the low Zn level of our Mg–Nd–Gd–Zn–Zr alloy according to Ref. [29]. Since the habit plane of the γ′ precipitate is on the basal Mg plane, these precipitates are not in contrast in the BF TEM images of Fig. 4a and c, which are along the $[01\bar{1}1]_{Mg}$ zone. After 90 min, small round features were also observed in the matrix, between the large platelets. Tilting experiments revealed these to be small dislocation loops.

3.4. Microstructural evolution during ECAP at 330 °C

The grain structure was less discernable in material subjected to 1-pass ECAP at 330 °C, as demonstrated in Fig. 5, however, a bi-modal grain size distribution was observed (not shown) and this is consistent with a large body of literature on ECAP processing Mg alloys whenever they contain coarse initial microstructures [30–32]. The mean grain size of the sample processed by ECAP for one pass was ~30 μm, which is nearly half the grain size of the AQ sample. When compared with the microstructure of the sample aged isothermally for 30 min, Fig. 3a and b, it was clear that the grain boundary precipitates (white contrast) were refined. Fig. 5a is an example of a large grain, similar to the grain size in the AQ condition. Inside these larger grains, elongated precipitates ~1 μm long were evident, Fig. 5b. Clear evidence of fragmentation of the β_1 precipitates was observed at high magnification after 1-pass ECAP, Fig. 5b. After 8-pass ECAP, the alloy retained the bi-modal grain size distribution although a mean grain size of 20 μm was measured, indicating a slight overall refinement. The degree of fragmentation of the β_1 precipitates was very extensive after 8 passes of ECAP, Fig. 5c.

Fig. 6 provides BF TEM micrographs and SAED patterns from samples processed by ECAP for 1-pass and 8-passes. In the 1-pass sample, fragmentation of a low number density of large β_1 particles was observed as indicated by a black arrow in Fig. 6a, which is consistent with that observed in the SEM images provided in Fig. 5b. In addition, a high number density of fine cuboidal precipitates of size range between 30 and 60 nm was evident. These fine cuboidal precipitates were unique to samples processed by ECAP. They formed via secondary precipitation induced by the 1-pass ECAP. Their distributions were uniform throughout the host matrix. Indexing the SAED along the $[01\bar{1}0]_{\alpha\text{-Mg}}$ zone from the 1-pass ECAP sample, Fig. 6b, confirmed that the small cuboidal precipitates were FCC β_1, and all had the same orientation relationship with the matrix, which is commonly reported in thermally aged Mg alloys [1–6]. After 8-passes of ECAP, spherical precipitates with a diameter of ~100 nm were observed in the finer grains of size ~0.5–1 μm, Fig. 6c. The size and morphology of these spherical precipitates at the boundaries and in the matrix were similar. The discontinuous nature of the corresponding ring-type SAED patterns, Fig. 6d, indicated that the microstructure consisted of both high angle and low angle grain boundaries. The weak reflection rings, marked with white dashed lines, were indexed as reflections

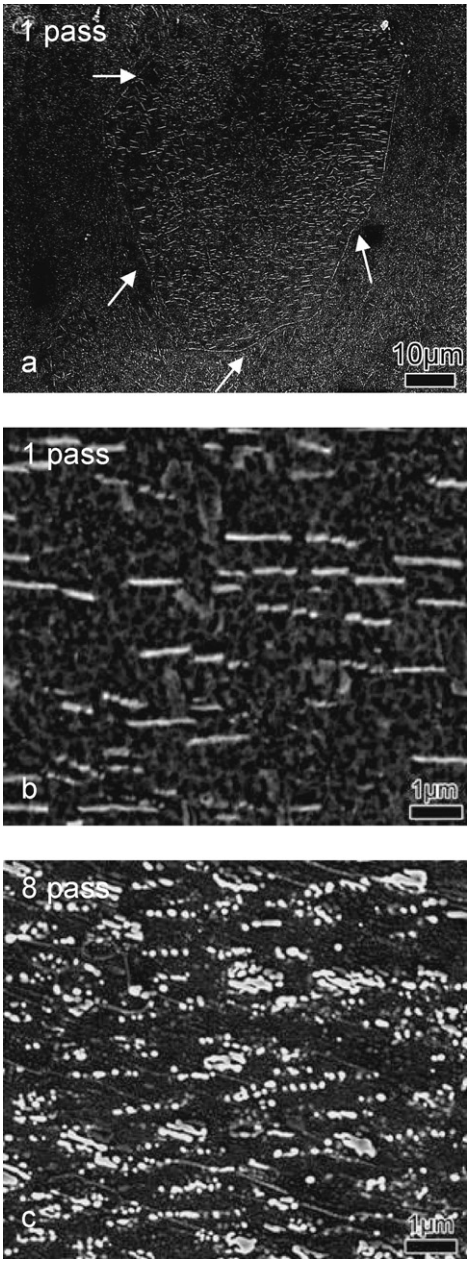

Fig. 5. Scanning electron micrographs of Mg–2.58Nd–1.80Gd–0.60Zn–0.15Zr alloy after ECAP at 330 °C: (a and b) 1 pass and (c) 8 passes, with white arrows pointed to grain boundaries.

from β_1 precipitates. The orientations of these β_1 precipitates were away from their initial preferred orientations as seen in the 1-pass ECAP sample (Fig. 6a).

4. Discussion

4.1. Precipitation in Mg–Nd–Gd–Zn–Zr alloy during isothermal ageing at 330 °C

The high-temperature ageing at 330 °C led to precipitation of β_1 and this is consistent with a precipitation sequence of SSSS → β_1 → β reported in a similar alloy aged at 300 °C [5]. The number density of these β_1 precipitates showed no clear decrease during ageing from 30 to 90 min, but the length of those large β_1 platelets increased during the time. Precipitation of hexagonal γ′ was identified during the isothermal ageing treatment, Fig. 4. These

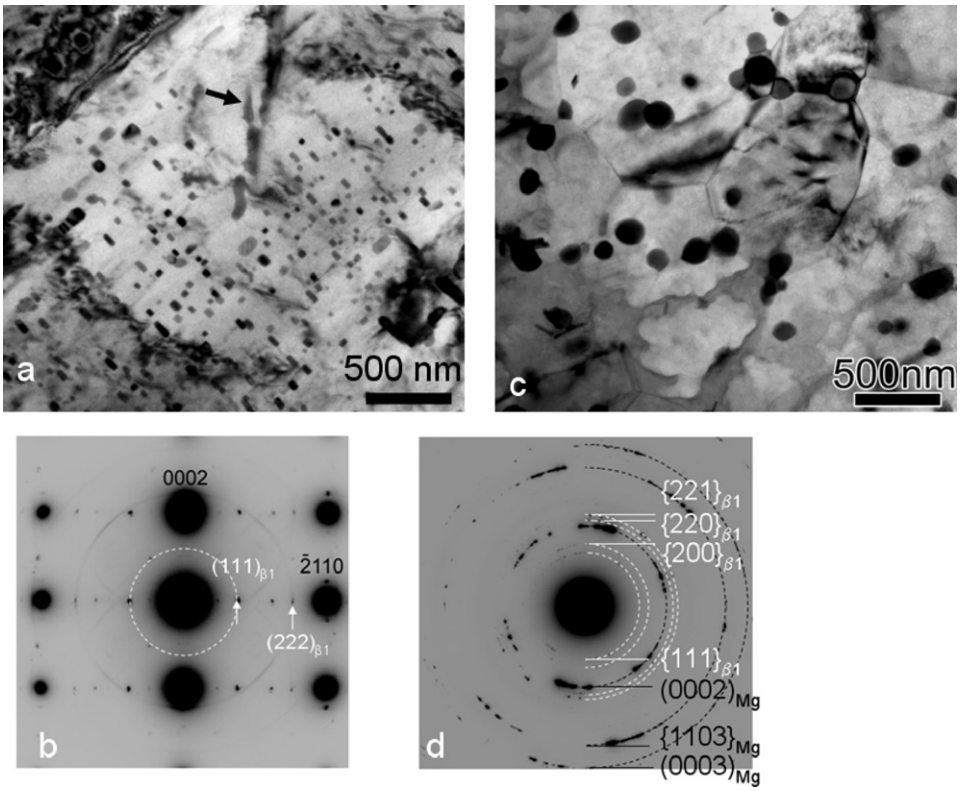

Fig. 6. TEM results from samples processed by ECAP at 330 °C (a) $[0\ 1\ \bar{1}\ 0]_{Mg}$ bright field image and (b) corresponding SAED pattern from alloy subjected to 1 ECAP pass. (c) Bright field image and (d) SAED pattern from alloy sample subjected to 8 ECAP passes.

metastable precipitates have been widely reported in similar Nd- and Zn-containing Mg alloys during ageing at high temperatures (>250 °C) [1,33]. They often form as platelets on the basal plane of the Mg matrix. It has been reported that prolonged thermal ageing will lead to the eventual replacement of γ′ precipitates by equilibrium γ (with an FCC unit cell similar to β_1) [1]. It is known that the basal γ′ platelets are less effective in serving as obstacles for basal slip than prism β_1 platelet precipitates in Mg alloys [34]. β_1 should be more effective to produce strengthening effect than γ′. Clearly, the softening effect observed from hardness measurements, as shown in Fig. 1, indicated that the precipitation of large β_1 precipitates in a low number density was insufficient to strengthen the alloy during isothermally ageing at 330 °C, but caused significantly softening of the matrix due to solute depletion in solution.

4.2. Precipitation in Mg–Nd–Gd–Zn–Zr alloy during ECAP at 330 °C

Precipitation of β_1 under ECAP at 330 °C follows the same sequence as that observed during isothermal ageing treatment at this temperature. The β_1 precipitates formed first, according to SAED analysis in Fig. 6b. The absence of γ′ reflections indicates that γ′ precipitation was suppressed under ECAP. The holding of samples for 15 min in a preheated die before ECAP at 330 °C led to the formation of a low number density of large primary β_1 precipitates habiting on the prismatic planes of the Mg matrix [6]. The 1-pass ECAP introduces a shear strain of ~1, and causes the fragmentation of some of the large precipitates (mostly ~1 μm in length) into smaller pieces, as show in Fig. 5b. 8-Pass ECAP introduced a total shear strain of ~8 and caused the fragmentation of the large primary platelets into many smaller equiaxed particles, as shown in Fig. 5c. Interestingly, these fragmented particles showed no clear increase in size, indicating that their growth have been suppressed effectively.

4.2.1. The nucleation of secondary β_1 precipitates

An important observation is that 1-pass ECAP promotes precipitation of small secondary β_1 precipitates (30–60 nm) in the Mg matrix already containing fragmented primary β_1 platelets, Fig. 6a. The number density of these secondary β_1 precipitates, as shown in Fig. 6a, is approximately two orders of magnitude higher than that in the sample isothermally aged at 330 °C, as shown in Fig. 4a. More interestingly, the orientation relationship between the secondary β_1 precipitates and the matrix, as shown in an SAED in Fig. 6b, is same as that commonly observed for β_1 in Mg alloys [5,8,35]. This suggests that these secondary β_1 precipitates likely formed during or after ECAP processing. Otherwise, the shear deformation under ECAP would cause rotation of the β_1 precipitates and make them deviate from their preferred orientation in the matrix. The rotation of precipitates has been reported in an Al–Zn–Mg–Cu alloy after 1-pass ECAP [25]. Prior to ECAP, the Al–Zn–Mg–Cu alloy initially contained fine precursor coherent precipitates in a high density and these transformed subsequently into η. This is different from the situation here with the Mg–Nd–Gd–Zn–Zr alloy which does not contain fine precursor precipitates for further transformation into secondary β_1, but only coarse primary β_1 precipitates in a low number density before ECAP. We believe that this is the explanation for the differing response of these two alloys after 1 pass of ECAP.

There are the well-known difficulties in homogenously nucleating β_1 precipitates in Mg alloys via conventional thermal ageing treatments [35]. The difficulties are likely related to local structural and compositional changes for nucleation of β_1. Since low-temperature precursor β″ has been found having the same stoichiometry Mg_3X as β_1 in Mg alloys during ageing in 200–250 °C range [6,36], the local structural change from the Mg lattice for the nucleation of β_1 is apparently more difficult to achieve. Recent investigations indicate that β_1 precipitates are fully coherent with the Mg matrix across their $\{1\ \bar{1}\ 0\ 0\}_{\alpha\text{-Mg}}$ habit planes, with an orientation relationship of $(\bar{1}\ 1\ 2)_{\beta_1}//(1\ \bar{1}\ 0\ 0)_{\alpha\text{-Mg}}$,

$[1\,1\,0]_{\beta_1}//[0\,0\,0\,1]_{\alpha\text{-Mg}}$, and a simple shear of magnitude ~0.22 on $\{1\,\bar{1}\,0\,0\}_{\alpha\text{-Mg}}$ plane in the $[\bar{1}\,\bar{1}\,2\,0]_{\alpha\text{-Mg}}$ direction is required for generating β_1 lattice from the α-Mg lattice [6]. In order to nucleate β_1 directly in the Mg matrix, a shear strain energy barrier has to be overcome to get the required structure transformation [6]. The shear strain introduced by 1-pass ECAP at 330 °C likely facilitated such structure transformation and promoted the nucleation of secondary β_1 precipitates in the α-Mg matrix. Depending on each grain orientation, the shear strain of 1 applied by 1-pass ECAP, may generate sufficient partial shear strain in $[\bar{1}\,\bar{1}\,2\,0]_{\alpha\text{-Mg}}$ direction on $\{1\,\bar{1}\,0\,0\}_{\alpha\text{-Mg}}$ plane to initiate the structure change to form β_1 nuclei. In addition, strain fields around dislocations could help to overcome the shear strain energy barrier for the nucleation of β_1, hence mobile dislocations introduced by ECAP probably assisted the heterogeneous nucleation of β_1. Because of a high processing temperature of 330 °C and a slow pressing speed of 5 mm/min, most dislocations were able to anneal out during ECAP, having β_1 precipitates left in the matrix, as shown in Fig. 6a and c.

4.2.2. The growth of secondary β_1 precipitates

Multiple passes caused the rotation of secondary β_1 precipitates formed during the 1-pass ECAP, as confirmed by a ring diffraction pattern from the 8-pass ECAP sample provided in Fig. 6d. The orientation change of the secondary β_1 precipitates resulted in the loss of their coherent interfaces with the Mg matrix lattices, and induced isotropic growth, rather than anisotropic growth widely observed in isothermally aged samples. As a result, β_1 particles grew into spherical morphology after 8-pass ECAP processing, as shown in Fig. 6c.

Fragmentation of large precipitates plays a major role in the evolution precipitate microstructure and this process is responsible for the spheroirdization of precipitates during ECAP [37]. However, fragmentation is less important for small precipitates evolution [25]. The fragmentation dominated the evolution of primary large β_1 precipitates (~1 μm), and restrained any significant growth of these broken primary β_1 particles in the Mg alloy during the 8 passes of ECAP processing, as seen in Fig. 5c. In contrast, a continues growth of the secondary precipitates were evident with the increase of the number of ECAP passes sample, as seen in Fig. 6c. This implied that fragmentation was not important for the evolution of secondary β_1 precipitates. Interestingly, secondary β_1 precipitates during ECAP processing showed much slower growth kinetics than the β_1 precipitates in the samples during isothermally ageing at the same temperature. For example, the size of large β_1 precipitates in the sample processed after 8-pass ECAP (170 ± 5 nm in diameter approximately, Fig. 6c) is significantly smaller than the size of large β_1 precipitates in the sample isothermally aged for 90 min (7 ± 0.05 μm long and ~100 nm thick in Figs. 3d and 4c). This is in great contrast with a rapid growth of η precipitates observed in Al–Zn–Mg–Cu alloy during ECAP [25].

In order to understand the interesting growth behaviours of secondary β_1 precipitates during ECAP, it is useful to have a look at the classic theory about the growth of an incoherent interface. The growth rate, v, can be expressed as follow [38],

$$v = K\ \Delta X_0 \sqrt{\frac{D}{t}}, \tag{1}$$

where $\Delta X_0 = X_0 - X_e$ is the supersaturation prior to precipitation, X_0 is actual matrix concentration, and X_e is equilibrium concentration of the matrix. D is the interdiffusion coefficient. K is a pre-factor, and t is time. Accordingly, ECAP should have a complicated effect on the growth of β_1 precipitates. On the one hand, ECAP introduces high-density dislocations, enhances interdiffusion for fast growth of precipitates. On the other hand, the dense secondary β_1 precipitates formed under ECAP have a mean interspacing of ~50 nm as shown in Fig. 6a, significantly shorter than that of ~500 nm in isothermally aged sample as seen in Fig. 4a. Consequently, diffusion fields of the dense secondary β_1 precipitates will overlap earlier, and causes a decrease of supersaturation ΔX_0 for slow growth of β_1. This second mechanism is more dominant than the first one and is responsible for the slow growth of high-density β_1 precipitates in the Mg-RE alloy processed by ECAP.

4.3. Hardening effect in Mg–Nd–Gd–Zn–Zr alloy processed by ECAP at 330 °C

Detailed microstructure characterization from this investigation confirmed that ECAP at 330 °C affected the microstructures of an Mg–Nd–Gd–Zn–Zr alloy in two aspects. Firstly, ECAP processing produced a limited grain refinement from an initial mean grain size of 50 μm (as-quenched) to 30 μm (1-pass) and 20 μm (8-pass). Secondly, ECAP processing promoted a significant precipitation of β_1 in a high number density in 1-pass sample, but caused the formation of coarse precipitates in 8-pass sample. A high hardness of 73 HVN measured in the 1-pass sample, above 63 HVN of the as-quenched sample, is consistent with the refined precipitate microstructure of 1-pass sample, hence, the hardening effect is likely due to combined strengthening of both precipitation and grain refinement. However, a decrease of hardness to 68 HVN observed in 8-pass sample clearly suggested that strengthening from the grain refinement from 30 to 20 μm was insufficient to compensate a softening due to the coarsening of precipitates in the alloy. Therefore, successful control of precipitate microstructure is essential for better strengthening effect in the Mg–Nd–Gd–Zn–Zr alloy.

This experimental investigation has demonstrated that high-temperature ECAP is effective to achieve precipitation strengthening in an Mg–Nd–Gd–Zn–Zr alloy. 1-Pass ECAP processing has promoted the uniform nucleation of a high density of β_1 precipitates. Multi-pass ECAP processing can cause the eventual coarsening of precipitates and reduced the strengthening effect, Fig. 1. The precipitation kinetics in the Mg–Nd–Gd–Zn–Zr alloy during high-temperature ECAP was clearly different from that observed recently in an Al–Zn–Mg–Cu alloy. A sluggish precipitation, i.e. about 1/100 of that in conventional ageing treatment (estimated from the volumes of large precipitates formed in both cases), was observed in the Mg alloy during ECAP at 330 °C. In order to obtain optimum strengthening from both grain refinement and precipitation hardening in the Mg alloy, a carefully designed ECAP procedure (reducing holding time, increasing pressing speed and lowering temperature) will be essential for better control of the precipitate microstructure and effective grain refinement.

5. Summary and conclusions

1. High-temperature ECAP is an effective route to modify precipitate microstructure to obtain precipitation strengthening in the Mg–Nd–Gd–Zn–Zr alloy, although it has no significant effect on the precipitation sequence in forming β phase, i.e. SSSS → β_1 → β, but the precipitation of γ′ was suppressed under the ECAP.
2. High-temperature ECAP effectively promotes the nucleation of dense β_1 precipitates, resulting in a marked strengthening effect, i.e. a ~19% increase of hardness above that of the as-quenched sample.
3. Holding the alloys at high temperature prior to ECAP caused precipitation of coarse primary β_1 precipitates. These became significantly fragmented with increasing number of ECAP passes.
4. Growth of β_1 precipitates during ECAP at 330 °C was much slower than that during isothermal ageing at the same temperature. This is mainly due to rapidly decelerating growth after the

diffusion field overlap from a high number density of precipitates formed under ECAP.

5. A combination of ECAP at 350 °C and a solution treatment can effectively modify the casting microstructures, homogenize chemical compositions, refine the mean grain size to 50 μm and reduce the presence of large particles at grain boundaries in the Mg–Nd–Gd–Zn–Zr alloy.
6. ECAP at 330 °C only produces a limited grain refinement with a mean grain size of 30 μm after 1 pass and 20 μm after 8 passes.

Acknowledgements

The authors are grateful for scientific and technical input and support from the Australian Microscopy & Microanalysis Research Facility (AMMRF) node at The University of Sydney, and the Australian Research Council with the ARC Centre of Excellence for Design in Light Metals. The assistance of Dr. Bulent Gun and Dr. Yanyan Sun on sample preparation and SEM analysis and the assistance of Dr. Xiaolin Wu and Mr. Jizhong Li on ECAP processing experiments are greatly acknowledged.

References

[1] P.A. Nuttal, T.J. Pike, B. Noble, Metallography 13 (1980) 3.
[2] B.L. Mordike, Mater. Sci. Eng. A 324 (2002) 103.
[3] J.F. Nie, X. Gao, S.M. Zhu, Scripta Mater. 53 (2005) 1049.
[4] J.F. Nie, K. Oh-ishi, X. Gao, K. Hono, Acta Mater. 56 (2008) 6061.
[5] L.R. Gill, G.W. Lorimer, P. Lyon, Adv. Eng. Mater. 9 (2007) 784.
[6] J.F. Nie, B.C. Muddle, Acta Mater. 48 (2000) 1691.
[7] I.J. Polmear, Light Alloys/Metallurgy of Light Metals, Metallurgy and Materials Science, 3rd ed., 1995, p. 96.
[8] C. Antion, P. Donnadieu, F. Perrard, A. Deschamps, C. Tassin, A. Pisch, Acta Mater. 51 (2003) 5335.
[9] P.J. Apps, H. Karimzadeh, J.F. King, G.W. Lorimer, Scripta Mater. 48 (2003) 475.
[10] R.Z. Valiev, R.K. Islamgaliev, I.V. Alexandrov, Prog. Mater. Sci. 45 (2000) 103.
[11] R.Z. Valiev, T.G. Langdon, Prog. Mater. Sci. 51 (2006) 881.
[12] Z. Horita, T. Fujinami, T.G. Langdon, Mater. Sci. Eng. A 318 (2001) 34.
[13] X.Z. Liao, F. Zhou, E.J. Lavernia, D.W. He, Y.T. Zhu, Appl. Phys. Lett. 83 (2003) 5062.
[14] X.Z. Liao, F. Zhou, E.J. Lavernia, S.G. Srinivasan, M.I. Baskes, D.W. He, Y.T. Zhu, Appl. Phys. Lett. 83 (2003) 632.
[15] Y. Huang, P.B. Prangnell, Acta Mater. 56 (2008) 1619.
[16] Y.M. Wang, Y.M. Chen, F. Zhou, E. Ma, Nat. Lett. 419 (2002) 912.
[17] Y.M. Wang, E. Ma, Acta Mater. 52 (2004) 1699.
[18] G.H. Zahil, Y. Huang, P.B. Prangnell, Acta Mater. 57 (2009) 3509.
[19] O.V. Mishin, A. Godfrey, Metall. Mater. Trans. A 39 (2008) 2923.
[20] H. Hasegawa, S. Komura, A. Utsunomiya, Z. Horita, M. Furukawa, M. Nemoto, Mater. Sci. Eng. A 265 (1999) 188.
[21] J. Wang, Y. Iwahashi, Z. Horita, M. Furukawa, M. Nemoto, R.Z. Valiev, T.G. Langdon, Acta Mater. 44 (1996) 2973.
[22] M. Murrayama, Z. Horita, K. Hono, Acta Mater. 49 (2001) 21.
[23] ZhaoYH, X.Z. Liao, Z. Jin, R.Z. Valiev, Y.T. Zhu, Acta Mater. 52 (2004) 4589.
[24] Y.H. Zhao, X.Z. Liao, S. Cheng, E. Ma, Y.T. Zhu, Adv Mater. 18 (2006) 2280.
[25] G. Sha, Y.B. Wang, X.Z. Liao, Z.C. Duan, S.P. Ringer, T.G. Langdon, Acta Mater. 57 (2009) 3123.
[26] Y. Iwahashi, J. Wang, Z. Horita, M. Nemoto, T.G. Langdon, Scripta Mater. 35 (1996) 143.
[27] M. Furukawa, Y. Iwahashi, Z. Horita, M. Nemoto, T.G. Langdon, Mater. Sci. Eng. A 257 (1998) 328.
[28] M. Yamasaki, M. Sasaki, M. Nishijima, K. Hiraga, Y. Kawamura, Acta Mater. 55 (2007) 6798.
[29] R. Wilson, C.J. Bettles, B.C. Muddle, J.F. Nie, Mater. Sci. Forum 419–422 (2003) 267.
[30] R. Lapovok, P.F. Thomson, R. Cottam, Y. Estrin, Mater. Sci. Eng. A 410–411 (2005) 390.
[31] R. Figueiredo, T.G. Langdon, Mater. Sci. Eng. A 501 (2009) 105.
[32] Q. Yang, A.K. Ghosh, Acta Mater. 54 (2006) 5147.
[33] X. Goa, J.F. Nie, Scripta Mater. 58 (2008) 619.
[34] J.F. Nie, Scripta Mater. 47 (2003) 1009.
[35] J.F. Nie, B.C. Muddle, Scripta Mater. 40 (1999) 1089.
[36] C. Anton, P. Donnadieu, F. Perrard, A. Deschamps, C. Tassin, A. Pisch, Acta Mater. 51 (2003) 5335.
[37] M. Murrayamma, Z. Horita, K. Hono, Acta Mater. 49 (2001) 21.
[38] D.A. Porter, K.E. Easterling, Phase transformations in Metals and Alloys, Nelson Thornes Ltd., UK, 2001, p. 279.